Journal of Fluorescence (2019) 29:387–398
https://doi.org/10.1007/s10895-019-02347-7

ORIGINAL ARTICLE

Aggregation Enhanced Excimer Emission Supported, Monomeric Fluorescence Quenching of Dendritic Hyperbranched Polyglycerol Coupled 1-Pyrene Butyric Acid Lumophore as a Sensing Probe for Fe_2O_3 Nanoparticles

Sherin Philip [1,2] · Sunny Kuriakose [1,2]

Received: 7 September 2018 / Accepted: 14 January 2019 / Published online: 13 February 2019

Abstract
Pyrene butyric acid (PBA) is a well studied lumophore for its exciting fluorescent properties. The current study focussed on a dendritic modification of PBA with hyperbranched polyglycerols (HPG) by Steglich esterification and further doping with iron oxide nanoparticles (IONP) of α-Fe_2O_3 phase. The covalent coupling between HPG and PBA was confirmed by FTIR and ^{1}H-NMR spectra. The main objective of the study was to monitor the fluorescent properties of the modified and doped products. Steady state PL emission studies showed a considerable decrease in fluorescence intensity on HPG modification which almost completely disappeared on doping with IONP. This suggests that this fluorosensing property can be explored in identification and estimation of iron oxide nanoparticles which has a great significance in biomedical field both in diagnostics and therapeutics. Lifetime measurements with TCSPC suggested an aggregation enhanced quenching of HPG-PBA conjugates and mixed static and dynamic mechanisms in IONP doped HPG-PBA conjugates.

Keywords PBA · HPG-PBA · HPG-PBA-IONP · Aggregation · Excimer · Quenching

Introduction

Fluorescence spectroscopy has grown into a promising detection and sensing tool. Fluorescent materials have been widely used for these purposes around the globe in various forms with wide ranging utilities. There are many fluorophores particularly organic ones with good fluorescence emissions that help to sense, identify or detect various elements of significance in the relevant area. Pyrene is a well established fluorophore for its excellent fluorescent emission properties, high sensitivity and rapid response time and is being studied for its applications in various fields. 1-pyrene butyric acid, a carboxylic derivative of pyrene is being used as an organic fluoro probe which finds its potential applications in biolabelling [1], biosensing [2], chemosensing, DNA-probing, protein detection and so on. Ever since the study of fluorescent pyrene butyric acid, its quenching by different quenching agents like various macromolecules has also been a topic of interest.

Pyrene is well known for its ability to form complexes with themselves. Pyrene usually with a structured emission at low concentrations, exhibit a peak around 440–480 nm at higher concentrations or in presence of a quencher, which may be attributed to excimer formation [3]. Functionalized and modified pyrene and its derivatives and their applications have been well studied for the past few decades. Pyrene butyric acid has been both covalently and non-covalently bonded to different macromolecular and supramolecular systems to investigate its complex formation potentials and the forthcoming applications. Of which, its modification with graphene layers is a well studied area. Hinnemo et al. [4] has covalently bonded graphene to pyrene butyric acid to have a possibility for π-π stacking interaction between the aromatic pyrene moieties and the graphene layers. Functionalized pyrene butyric acid has been made use in various types of sensing technologies [5] by means of modification to physical and chemical properties of the analytes [6, 7]. PBA/graphene composites were prepared by immobilization of

✉ Sunny Kuriakose
skresearchgroup16@gmail.com; sherinphilip.m@gmail.com

[1] Department of Chemistry, St. Thomas College, Palai 686574, India

[2] Mahatma Gandhi University, Kottayam, Kerala, India

pyrene on graphene sheets by means of π-π stacking to study their electrochemical properties [8].

Pyrene butyric acid is being rigorously studied for its outstanding photoluminescent properties. Various macromolecular and supramolecular modifications of PBA have been carried out to inquire their effect on the photoluminescence of the latter. Li et al. has developed a water-soluble pyrene-containing fluorescent polymer by click reaction between thiol and a carbon-carbon double bond [9]. A temperature and concentration based research on PBA embedded in polymethyl methacrylate (PMMA) was conducted by Ara et al. [10]. Fluorescence depolarization studies were conducted on PBA-bovine serum albumin conjugates to study the properties and configuration of proteins [11]. At the same time pyrene modified systems have been studied for their sensing capacities for various elements of interest in the relevant fields.

Quantitative fluorescence decay studies of pyrene labelled macromolecules and supramolecules have been conducted for identification and better characterization of these molecules and to understand their biomedical applications at a greater depth [12]. The kinetics of excimer formation in pyrene-labeled macromolecules is well described by a modified version of the original Birks′ scheme [1, 13, 14]. Pyrene excimer formation contrasts with other photophysical processes used to probe macromolecules such as electron transfer (ET) [15] or fluorescence resonance energy transfer (FRET). The unusual retention of excess energy by the pyrene chromophore is a consequence of the absence of overlap between its absorption and fluorescence spectra. At extremely low concentrations and if both the macromolecule and pyrenyl label are well-solvated, an excited pyrene label covalently attached to a macromolecule decays to the ground state before forming an excimer intermolecularly with a ground-state pyrene, thus easily enabling the quantitative identification of the macromolecule. Temperature and concentration dependence of PBA in a PMMA film was studied with the help of electric field modulated (EF) spectra by Ara et al. [10].

One of the prominent areas of research where PBA probes have been used is of course the DNA sensing. Molecular oxygen quenching of PBA has been strongly explored to monitor oxygen levels in cellular components which can be used for their probing or sensing studies. O_2 sensing [16] capability of PBA makes it a useful probing tool in studies related to segmented flexibility of proteins [17], fluidity of membranes [18] and association of polymers [19–22]. An optical oxygen-sensing material based on the fluorescence intensity changes of pyrene-1-butyric acid (PBA) chemisorption film has been developed and characterized by Fujiwara et al. [23].

Quenching can be any phenomenon that is responsible for the decrease in fluorescence intensity of the fluorophore and can be of static or dynamic origin. Static quenching arises when a fluorophore and a quencher forms a non-fluorescent complex in the ground state before excitation and is accompanied by no significant change in fluorescence lifetime [3, 24]. Whereas in dynamic quenching a complex formation takes place after excitation of the fluorophore as a result of an energy transfer between the quencher and the fluorophore. Fluorescence lifetime is considerably reduced in dynamic quenching with an appreciable decrease in luminescence intensity. The particles that undergo static quenching are “dark”. The extent of static quenching is therefore simply related to the fraction of the particles having either a deep carrier trap or an adsorbed quencher that very rapidly quenches the excited state [25, 26].

Fluorescence Resonance Energy Transfer (FRET) is an inevitable term wherever quenching of fluorescence is discussed. It is a distance-dependent physical phenomenon in which an excited donor fluorophore molecule transfers the excitation energy to a nearby chromophore, which is the acceptor molecule that can either be fluorescent or non-fluorescent. In FRET, energy transfer manifests itself through decrease or quenching of the donor fluorescence and a reduction of excited state lifetime accompanied also by an increase in acceptor fluorescence intensity. For a FRET process to occur the donor and acceptor molecules must be in close proximity, preferably between 1 and 10 nm. Moreover, the absorption or excitation spectrum of the acceptor must overlap the fluorescence emission spectrum of the donor. The degree to which

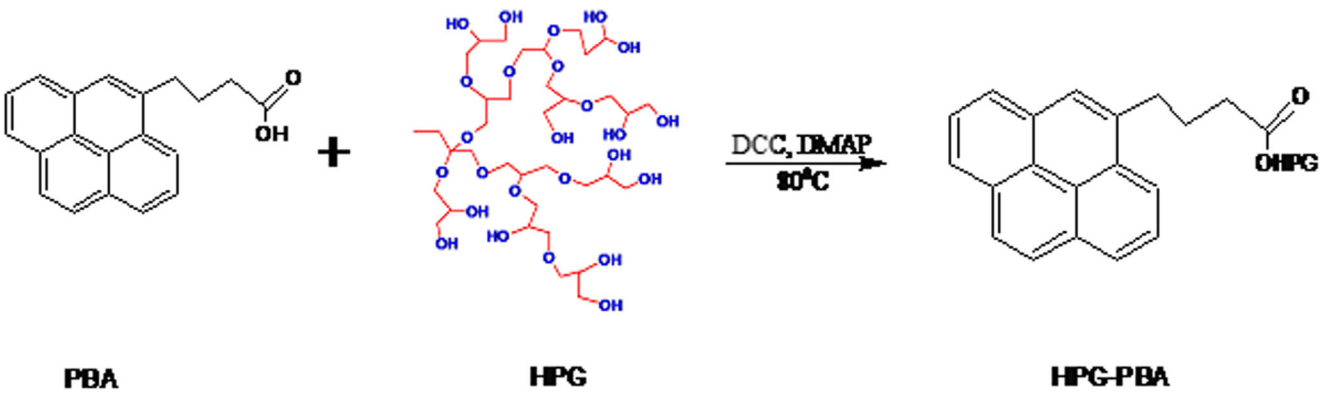

Scheme 1 Synthesis of HPG-PBA conjugate by Steglich esterification

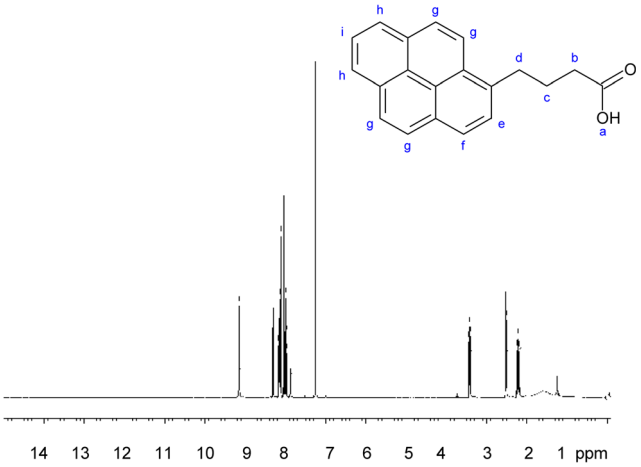

Fig. 1 ^{1}H-NMR spectrum of pyrene butyric acid (PBA)

they overlap is referred to as the spectral overlap integral (J). The donor and acceptor transition dipole orientations must be approximately parallel. Förster [27] showed that the efficiency of the FRET process (E) depends on the inverse sixth power of the distance between the donor and acceptor pair (r) and is given by

$$E = R_0^6/\left(R_0^6 + r^6\right) \quad (1)$$

Where R_0 is the Förster radius at which half of the excitation energy of donor is transferred to the acceptor chromophore. Therefore Förster radius (R_0) is referred to as the distance at which the efficiency of energy transfer is 50%.

Over the past few decades, a novel category of highly branched macromolecules called dendrimers has received much attention due to their potential applications [28–31]. Aggregation enhanced emission of pyrene based dendrimers has already been reported [32]. Aggregation enhanced emission of a pyrene-phosphonate conjugate has been made use in sensing Fe^{3+} ions selectively [33]. In the present study pyrene butyric acid was immobilized on dendritic hyperbranched polyglycerol (HPG) by DCC coupling between the two, establishing a covalent interaction and further doped with α-Fe_2O_3 nanoparticles to study their quenching effect on the PBA luminescence.

A deeper detailed understanding of the quenching mechanism was drawn with the help of time correlated single photon counting (TCSPC) for lifetime measurements. TCSPC outperforms all other techniques in sensitivity, dynamic range, data accuracy and precision. Since TCSPC measures single photons, detection is at the quantum limit. The technique requires an excitation source with high repetition rate pulsed output. As the process of capturing a single photon is repeated several thousand or even a million times per second, a sufficiently high number of single photons is processed for the resulting fluorescence lifetime measurement. Only one photon is processed at a time, so the light pulses required for sample excitation have low pulse energy, which causes minimal sample degradation and avoids many non-linear sample effects.

Experimental

Materials

Hyperbranched polyglycerol (HPG, m.w-5000) was obtained from the research group of Prof. Holger Frey of Johannes-Gutenberg University, Mainz, Germany.

1-pyrene butyric acid (PBA, 97%), 4-dimethyl aminopyridine (DMAP, 99%), N,N′-dicyclohexyl carbodiimide (DCC, 99%), dimethyl formamide (DMF, 95%) and all other solvents were purchased from Sigma-

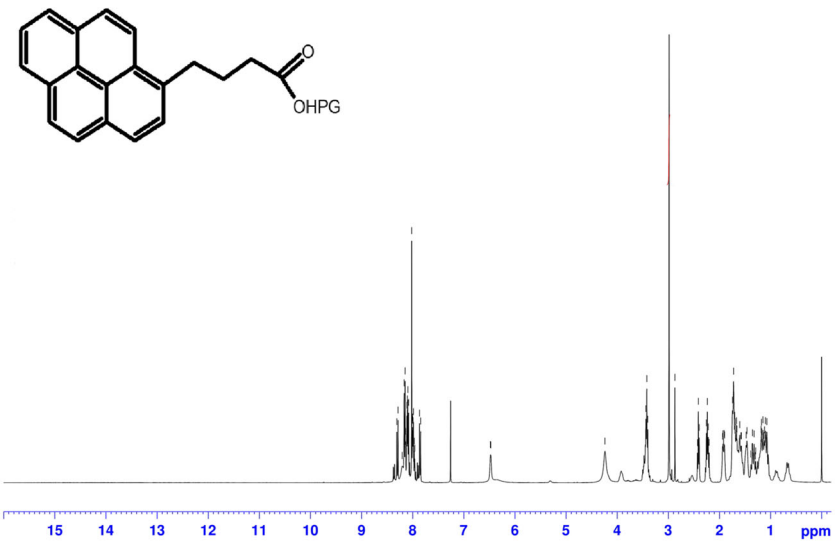

Fig. 2 ^{1}H-NMR spectrum of HPG-PBA aggregates

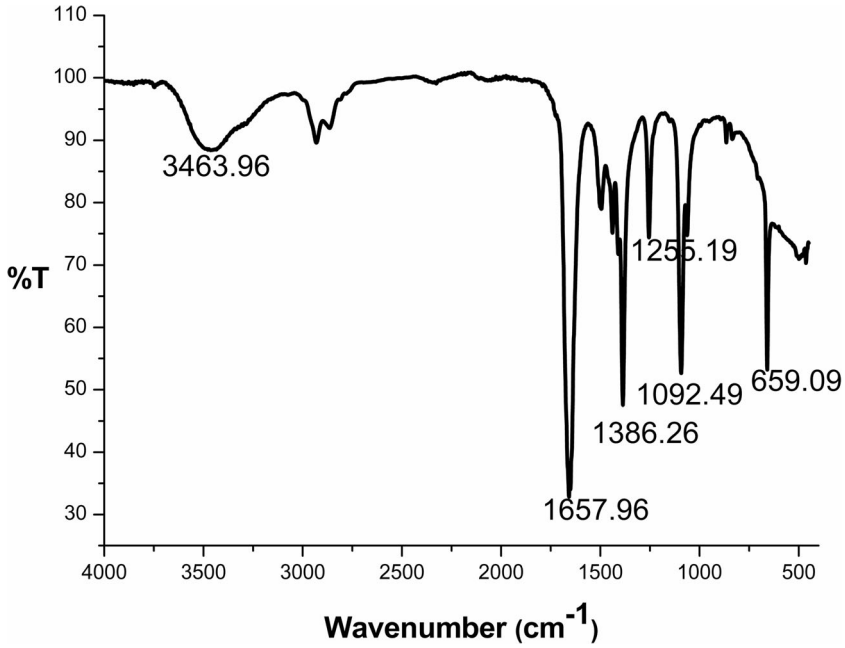

Fig. 3 FTIR spectrum of HPG-PBA aggregates

Aldrich and used without any further purification. Ferrous sulphate heptahydrate ($FeSO_4.7H_2O$, 99%) and sodium borohydride ($NaBH_4$, 98%) for the synthesis of α-Fe_2O_3 nanoparticles were obtained from HiMedia Pvt.Ltd., India.

Instrumentation

A Bruker Avance NMR spectrometer (^1H, 500 MHz) was used to characterize the synthesized samples in $CDCl_3$ with the chemical signals referenced to solvent residual signal in ppm. FTIR spectrum was recorded on a Shimadzu-400 FTIR spectrophotometer in the range 400–4000 cm^{-1}. The crystalline properties of the α-Fe_2O_3 nanoparticles were studied using Rigaku Miniflex 600 XRD instrument operating at 1.54 A^0 with a CuKα source.

Microscopic studies were done using JEOL Model JSM - 6390LV scanning electron microscope (SEM) and Jeol/JEM 2100 high resolution transmission electron microscope (HRTEM) operating at 200 kV. Sample for SEM analysis was mounted on an electrically conductive carbon stub appropriate for the particular scanning electron microscope being used. More detailed microscopic study was conducted using high resolution transmission electron microscope (HRTEM), which uses a LaB6 source. The sample dispersion in alcohol is made into a thin film by ultramicrotomy so that the electrons can easily be transmitted through the very thin sample. The ultra thin sample section is mounted on supporting mesh grids. Images were captured with a side mounted digital camera AMT XR40. Grids used in the experiment were 200 mesh copper grids carbon coated.

The optical properties were monitored using UV/visible and photoluminescence spectroscopic techniques. All spectra were recorded in DMF at room temperature. Absorption spectra for each sample were recorded on a Shimadzu UV/visible spectrophotometer in the range 190–1100 nm.

Photoluminescence studies were conducted using a Horiba Flouorolog-3- spectrofluorometer with an excitation wavelength at 295 nm with a band pass of ±5 nm. Measurements were carried out with 3 nm emission slits, using 1.25 × 4.5 cm quartz cuvettes, containing 3.5 ml of solution. Steady-state fluorescence emission spectra were collected from 305 to 550 nm, excited with a Broadband 450-W CW Ozone-free xenon arc lamp at 295 nm. The beam was concentrated on the sample either directly or by means of a reflecting objective (74X). All emission spectra were uncorrected. Lifetime measurements were recorded using time correlated single photon counting (TCSPC) technique. The samples were excited using PLS(295) LED diode and the photons were counting until at least 10,000 counts were collected at the maxima of the fluorescence decay histograms. After collection of the emitted photons on a photomultiplier (Photomultiplier R928P), the signal is digitized with a numerical oscilloscope. The raw data were analyzed by a multi-exponential model with reconvolution of the instrument response function (IRF). Reconvolution of

Scheme 2 Synthesis of HPG stabilised IONP

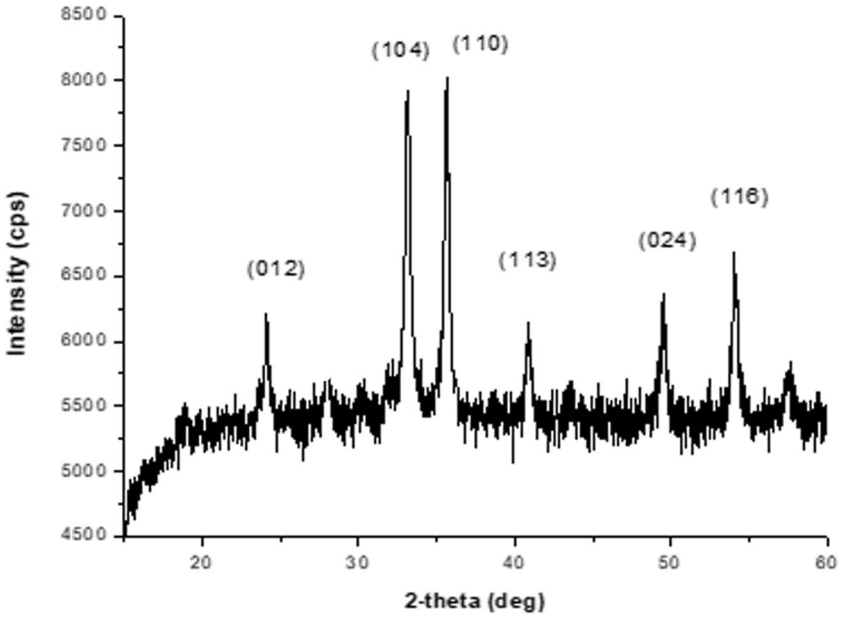

Fig. 4 XRD pattern of HPG stabilised IONP

fluorescence decay curves was performed using HORIBA Scientific decay analysis DAS6 software. In our study, we observed only double exponential lifetime decay.

The single-photon pulses from the avalanche photodiode are fed to the input DETECT. To avoid an influence of amplitude jitter of the detector input pulses a constant fraction discriminator (CFD) is used to provide a well defined start pulse for the time-to-amplitude converted (TAC). The synchronization signals (stop pulse) generated by the pulse generator of the laser diode are fed to the input SYNC. To improve the timing of the synchronization signal also, the SYNC circuit contains a CFD. In addition, an adjustable frequency divider with ratios from 1:1 to 1:16 is implemented. Divider ratios greater than one can be used to record several periods of the light signal.

Synthesis and Characterization of Hyperbranched Polyglycerol Coupled Pyrene Butyric Acid Conjugates (HPG-PBA)

HPG-PBA conjugates were synthesized following a modified Steglich esterification [34] by DCC coupling (Scheme 1). Hyperbranched polyglycerols (0.13 g) and pyrene butyric acid (0.5 g) in 10 ml DMF each were mixed together followed by addition of 10 ml DCC (0.5 g) in DMF. HPG and PBA were mixed in the prescribed weights inorder to maintain a 1:1 M ratio between the –OH groups of HPG and –COOH groups of PBA. HPG (m.w. 5000) contains 68 hydroxyl groups so that a single HPG dendritic molecule can be coupled with 68 molecules of PBA. A catalytic amount of DMAP (200 mg) was added and the mixture was stirred at room temperature for 2 h and then at 80 °C for 6 h under nitrogen flushing. The mixture was then cooled to room temperature and then freezed at -25 °C and filtered to remove the reaction byproduct dicyclohexyl urea (DCU) and all the unreacted molecules. The solvent was evaporated using a rotary flash evaporator and the product was allowed to dry at room temperature in vacuum.

Esterification between the carboxylic acid (-COOH) group of PBA and hydroxyl (OH) groups of HPG establishes a covalent bonding between the fluorophore and the dendrimer.

The coupled product is characterized by ^{1}H-NMR spectroscopy (Fig. 2) and compared with that of unmodified PBA (Fig. 1) to confirm the presence of an ester linkage.

Table 1 X-ray diffraction data

Peak Position (2θ in degrees)	Full Width at Half Maximum, FWHM (degrees)	Crystallite Size $d = {}^{K\lambda}/_{\beta cos\theta}$ (nm)	Crystal plane
24.05	0.49	17.32	(012)
33.152	0.40	21.65	(104)
35.611	0.326	26.74	(110)
40.81	0.39	22.71	(113)
49.43	0.36	25.38	(024)
54.05	0.41	22.73	(116)

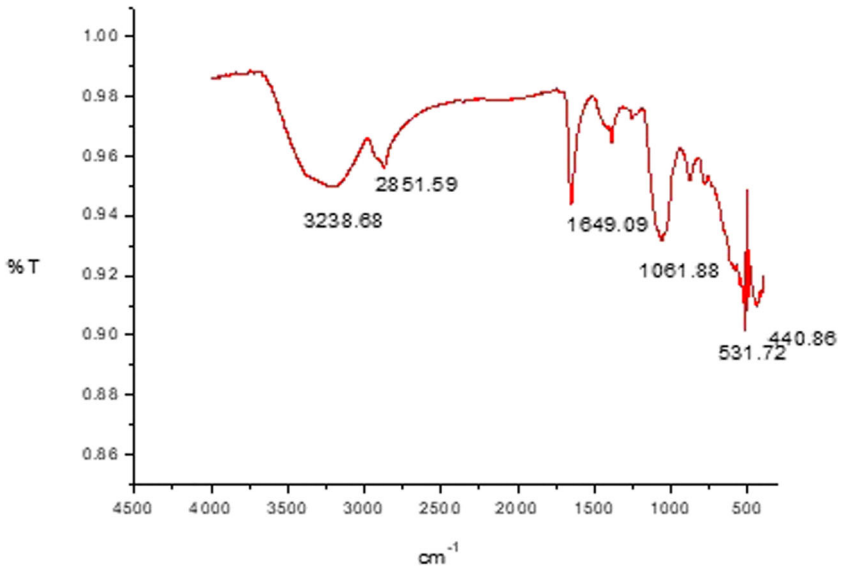

Fig. 5 FTIR spectrum of HPG stabilised IONP

^{1}H NMR spectrum of pyrenebutyric acid (Fig. 1): δ 9.16 ppm (1H, s, -COOH proton 'a'), δ 7.8–8.3 ppm (aromatic protons of pyrene), δ 3.44 ppm (2H, t, aliphatic protons 'b'), δ 2.53 ppm (2H, t, aliphatic protons 'd'), δ 2.25 ppm (2H, m, aliphatic protons 'c') and δ 7.3 ppm ($CDCl_3$ solvent).

^{1}H NMR spectrum of HPG-PBA (Fig. 2): δ 7.84–8.3 ppm (aromatic protons of pyrene), δ 3.41 ppm (2H, t, aliphatic protons 'b'), δ 2.9 ppm (1H, s, COOR-CH- proton ester), δ 2.4 ppm (2H, t, aliphatic protons 'd'), δ 2.23 ppm (2H, m, aliphatic protons 'c'), δ 1–2 ppm (aliphatic protons of HPG) and δ 7.3 ppm ($CDCl_3$ solvent).

The absence of any peak corresponding to –COOH proton in the nmr spectrum of coupled HPG-PBA product (Fig. 2) indicates the complete conversion of carboxylic groups of PBA to ester linkages. The formation of ester is further confirmed by a sharp peak at 2.9 ppm corresponding to α-hydrogens in HPG bonded to –COOR group. As there are 68 hydroxyl groups in an HPG molecule (m.w.5000), a single HPG molecule can be coupled with 68 molecules of PBA each bearing a single –COOH group. Thus such a great number of PBA molecules find themselves in a close proximity on a dendritic platform, which makes the dimer formation more easy compared to free PBA molecules. A weak band at 6.4 ppm may be due to the presence of dicyclohexyl urea (DCU) which is the major byproduct of the coupling reaction.

FTIR spectrum of HPG-PBA conjugates (Fig. 3) was recorded as KBr discs in the frequency range 4000–400 cm^{-1}. IR(KBr): 3463.96 cm^{-1}: ν_{O-H} (str), 1657.96 cm^{-1}: $\nu_{C=O}$ (str), 1386.26 cm^{-1}: ν_{C-H} (bend), 1255.19 cm^{-1}: $\nu_{O=C-O-C}$ (str) of esters, 1092.49 cm^{-1}: ν_{C-O-C} (str) of ethers and 659.09 cm^{-1}: ν_{C-H} (bend).

The peaks at 3463.96 cm^{-1} due to hydroxyl stretching and that at 1092.49 cm^{-1} due to ether group indicates the presence of hyperbranched polyglycerol in the conjugate whereas those at 1657.96 cm^{-1} and 1255.19 cm^{-1} corresponding to carbonyl and ester groups confirms the ester linkage formed between HPG and PBA. Therefore, the NMR and FTIR spectra of the coupled product could undoubtedly claim the successful covalent bonding through ester linkage between the dendrimer HPG and the fluorophore PBA.

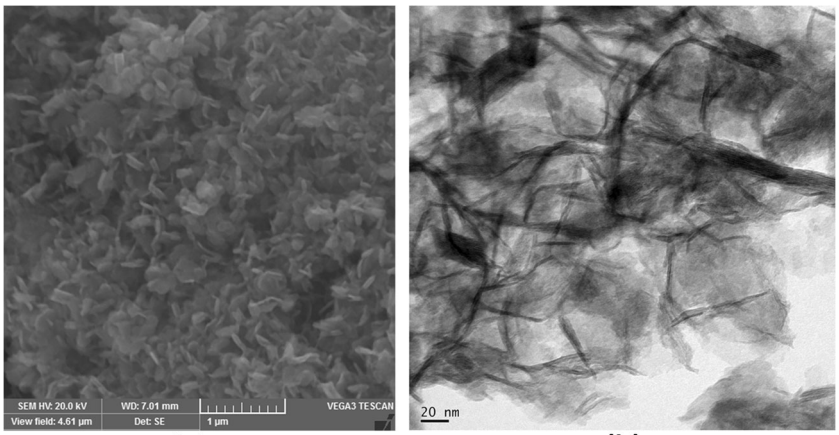

Fig. 6 **a** SEM and **b** HRTEM images of HPG stabilised IONP

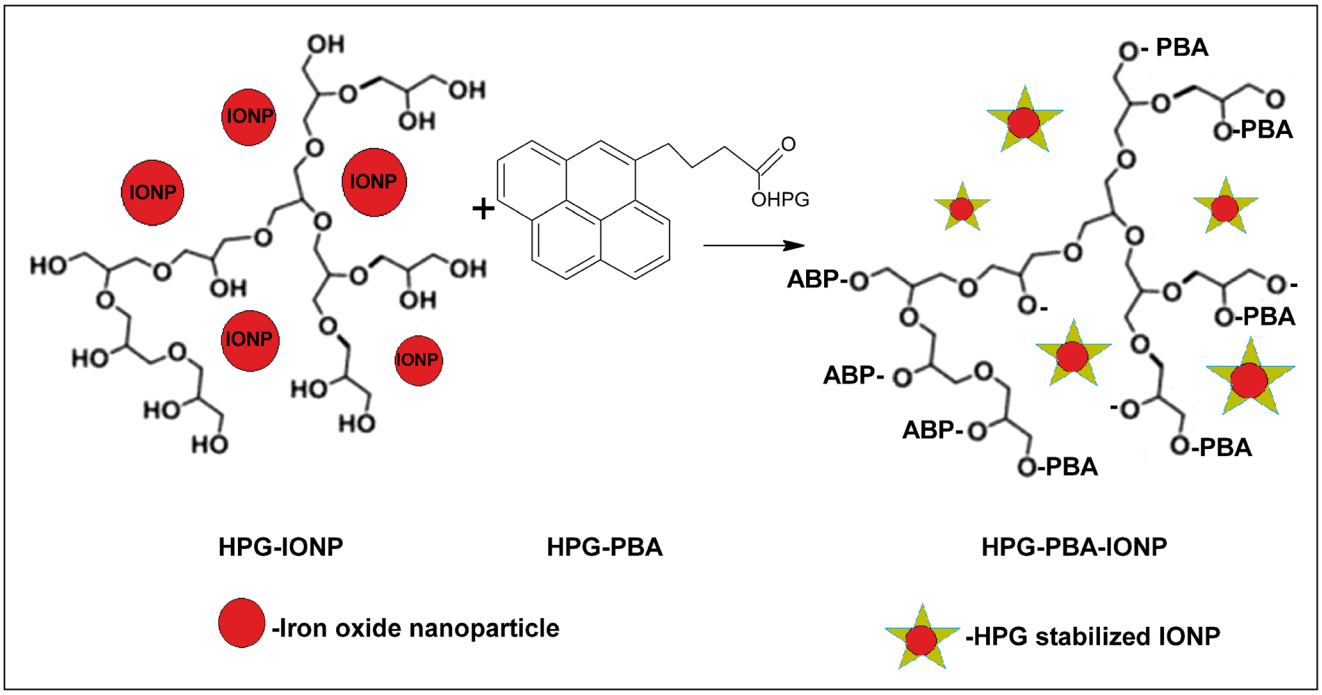

Scheme 3 Synthesis of HPG-PBA-IONP aggregates

Synthesis and Characterization of Hyperbranched Polyglycerol Stabilized α-Fe_2O_3 Nanoparticles (IONP)

HPG stabilized iron oxide nanoparticles were prepared by well established $NaBH_4$ reduction–oxidation protocol. Aqueous solutions of 0.001 M HPG (0.125 g, 25 ml) was magnetically stirred under nitrogen atmosphere into which 0.03 M $FeSO_4.7H_2O$ (.208 g, 25 ml) was added dropwise and stirred further for 4 h at 25 °C as reported elsewhere [35]. 0.3 M $NaBH_4$ (0.1135 g, 10 ml) was added vigorously and stirred again for 30 min. The black Fe(0) was filtered, washed with ethanol (99%). Reduced zero-valent iron was then subjected to air oxidation at 200 °C for 1 h and the oxidized α-Fe_2O_3 nanoparticles were collected and stored under vacuum at 25 °C.

Scheme 2 describes the synthesis of α-Fe_2O_3 nanoparticles stabilized in the dendritic architecture of hyperbranched polyglycerol by $NaBH_4$ reduction followed by oxidation. HPG was used to encapsulate the nanoparticles to make it more hydrophilic and polar.

The crystalline properties and size of IONPs were determined by XRD analysis as given in Fig. 4. The peak indexing indicates the presence of α-Fe_2O_3 only and no other phases of iron oxides were present. The crystallite size was calculated using Debye-Scherrer equation $d = {}^{K\lambda}/_{\beta cos\theta}$ and found to be in the range 17–26 nm, where K = 0.94 is the shape factor, λ = 1.54A^0 is the wavelength of x-ray used. All other parameters are listed in Table 1.

A more insight into the bonding nature of the synthesized nanoparticles was drawn by recording the FTIR spectrum (Fig. 5). HPG stabilized Fe_2O_3 nanoparticles IR(KBr): 3238.68 cm^{-1}: ν_{O-H} (str), 2851.59 cm^{-1}: ν_{C-H} of CH_2,

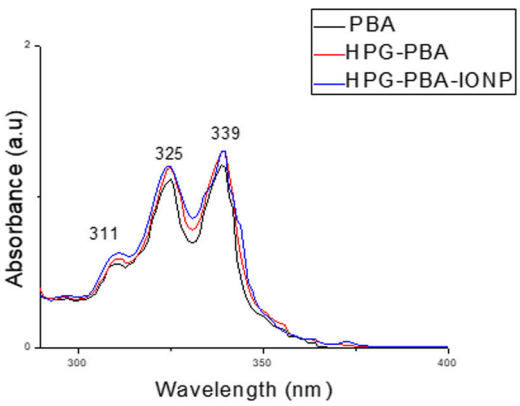

Fig. 7 UV/visible absorption studies

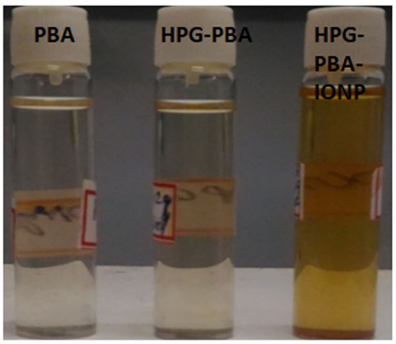

Table 2 Absorption intensities

Sample/Absorption intensity	311 nm	325 nm	339 nm
PBA	0.553	1.112	1.206
HPG-PBA	0.590	1.187	1.304
HPG-PBA-IONP	0.630	1.201	1.304

1649.09 cm^{-1}: $\nu_{H\text{-}O\text{-}H}$ (bend), 1061.88 cm^{-1}: $\nu_{C\text{-}O}$ (str), 531.72 and 440.86 cm^{-1}: $\nu_{Fe\text{-}O}$ (str).

The two peaks below 600 cm^{-1} indicates Fe-O bonds in Fe_2O_3 [36–38] and those others indicate the presence of the dendrimer.

The surface topography and morphology of the sample was studied using SEM (Fig. 6a) and a detailed microscopic study of the particle was done using HRTEM imaging technique (Fig. 6b).

The hexagonal geometry of α-Fe_2O_3 is clearly understood from the SEM image and the high resolution TEM image vividly reveals the encapsulation of iron oxide nanoparticles into the dendritic architecture. SEM images show hexagonally shaped crystals of α-Fe_2O_3 nnaoparticles. In HRTEM image the black streaks of α-Fe_2O_3 nanoparticles seem to be well embedded in the dendritic framework of HPG.

Synthesis of IONP Doped HPG-PBA Conjugates (HPG-PBA-IONP)

Dispersions of HPG-PBA conjugate (0.010 g, 10 ml) and HPG stabilized IONP (0.010 g, 10 ml) in DMF were mixed thoroughly and magnetically stirred for 1 h at 80 °C and further for 4 h at 25 °C under nitrogen flushing. The solvent was evaporated using a rotary flash evaporator and the product was dried at room temperature in vacuum. The product was purified using column chromatography with 8:2 (*v*/v) acetonitrile-methanol solvent system on a 100–200 mesh silica (Merck India Pvt.Ltd.) filled 2 × 20 cm adsorption column.

HPG stabilized α-Fe_2O_3 nanoparticles were efficiently incorporated into the HPG-PBA conjugates by stirring both solutions in DMF (Scheme 3). The significance of encapsulation of IONP into HPG lies here because the dispersion can be efficient if both solutions are in the same phase and the highly hydrophilic HPG makes IONP more dispersible in a polar solvent like DMF. Moreover, the presence of HPG in both nanoparticles and the lumophore makes them more miscible and compatible with each other. Thus the HPG coating of IONP makes them easily diffusible into the HPG-PBA conjugates.

Results and Discussions

UV/Visible Absorption Studies

UV/visible absorption spectrum (Fig. 7) was recorded for PBA, HPG-PBA and HPG-PBA-IONP samples in DMF in equal molar concentrations at room temperature, to monitor the effect of dendritic and nano-modification of the pyrene moiety on its absorption properties. The absorption spectra of all the three samples showed three peaks in the UV region with an ascending order of increasing intensity with increasing wavelength. The two prominent peaks at 325 nm and 339 nm can be attributed to the S_0-S_2 transition of pyrenyl chromophores [39, 40]. All the three samples exhibited absorption

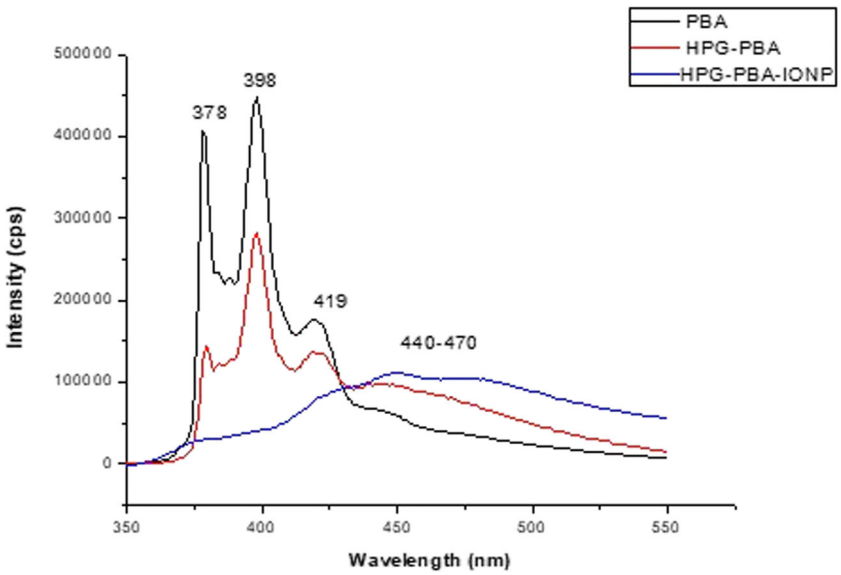

Fig. 8 Steady state PL emission

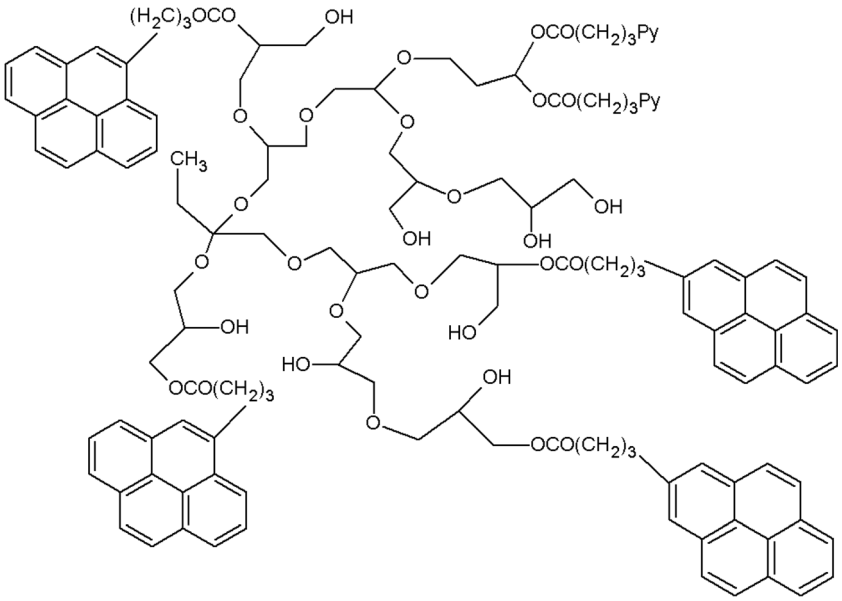

Fig. 9 Schematic representation of possible aggregation of pyrene molecules on the dendritic platform of HPG

curves of almost similar shapes but slightly increased intensity (Table 2). No considerable shift either blue or red is observed on modification of the fluorophore with the dendrimer or IONP. It is clear that the colour of HPG-PBA-IONP aggregates considerably changed to yellowish brown on encapsulation of iron oxide nanoparticles (Fig. 7). This colour change indicates the efficient non-covalent interaction of α-Fe_2O_3 nanoparticles with the dendrimer-modified fluorophore.

Steady State Fluorescence Emission Studies

Steady state fluorescence emission studies of the samples were conducted in DMF at an excitation wavelength of 295 nm at room temperature, at equal molar concentrations

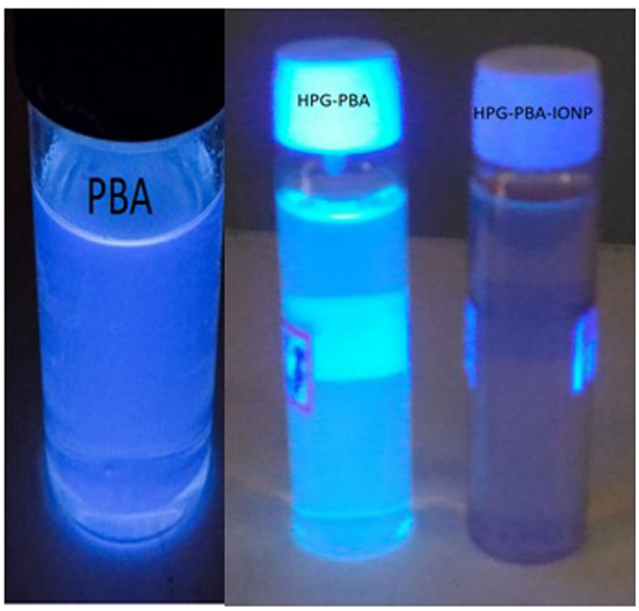

Fig. 10 Emission upon UV irradiation

(Fig. 8). The two intense peaks at 378 nm and 398 nm of pure PBA are characteristic of pyrene monomers and a considerably weak peak near 440 nm indicates a negligible amount of pyrene as dimers in the excited state (excimers). While when PBA is dendritically modified by covalent ester coupling to hyperbranched polyglycerols via Steglich esterification, the peaks corresponding to pyrene monomers get considerably reduced in intensity and that of pyrene excimer get intensified, which indicates the formation of excimers on modification. This quantitative increase in excimer formation may be attributed to aggregation of pyrene monomers on the dendritic HPG platform. HPG (obtained from Frey's group) synthesized by ring opening multi-branching polymerization (ROMBP) of glycidols [41], is having many hydroxyl groups which get esterified on coupling with PBA. Thus HPG forms a dendritic platform for the pyrene monomers to get aggregated at a close proximity (Fig. 9). Thus the formation of excimers efficiently quenches the PL emission of pyrene monomers.

It's quite interesting to note that the PL emission of HPG-PBA conjugates further get significantly decreased on interaction with α-Fe_2O_3 nanoparticles. The monomer emission is almost absent with a characteristic excimer peak near 470 nm, characteristic of pyrene excimer. Besides, it's important to note that the excimer emission is red shifted than the HPG-PBA conjugates on addition of Fe_2O_3 nanoparticles, which is a clear indication of the interaction of nanoparticles with the dendrimer-fluorophore system.

The quenching of fluorescence is evidently seen from the emission differences in UV irradiated samples of PBA and its modified analogues in DMF at room temperature. PBA has an intense blue emission whereas upon dendritic modification with HPG the emission changes to a green tinted one which justifies the red shifted excimer formation in the PL spectrum of HPG-PBA conjugates

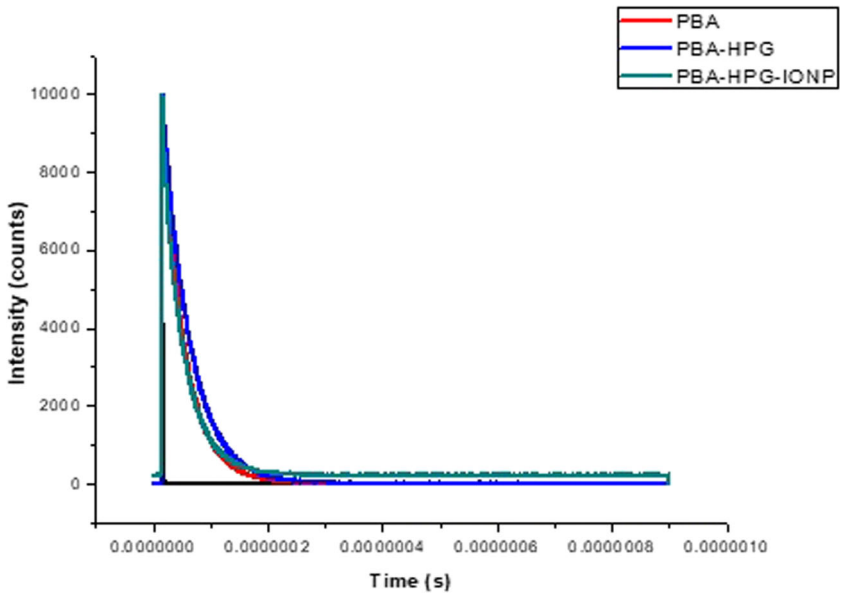

Fig. 11 PL decay curves as a function of time

(Fig. 10). Also, the IONP added sample had no significant monomer emission which confirms almost a complete quenching of the fluorescence of the fluoroprobe. This modification can thus be used as a naked eye detection technique for the presence of iron oxide nanoparticles in a system under study. This is important since iron oxide nanoparticles are potentially useful candidates in the area of medicine as a theranostic agent, particularly in imaging techniques like MRI contrasting.

Time Correlated Single Photon Counting for Lifetime Analysis (TCSPC)

Time-resolved fluorescence spectroscopy is used for the life time analysis of the samples under consideration in the current study. With periodic excitation from a laser, it is possible to extend the data collection over multiple cycles of excitation and emission in time correlated single photon counting (TCSPC). One can then accept the sparseness of the collected photons and reconstruct the fluorescence decay profile from the multitude of single photon events collected over many cycles. The method is based on the repetitive, precisely timed registration of single photons [3, 42]. The reference for the timing is the corresponding excitation pulse. Besides, it gives us a clear cut idea about the mechanism that prevails in the quenching process, whether static or dynamic. In the present study, lifetime measurements of PBA, HPG-PBA and HPG-PBA-IONP samples were recorded in DMF at room temperature using TCSPC measurements and the decay curves are plotted in Fig. 11. All samples were observed to exhibit double exponential decay only.

The average lifetime was calculated using the equation $\tau_{av}=\frac{a1\tau1+a2\tau2}{100}$, where a_1 and a_2 are the normalized amplitudes of the components and τ_1 and τ_2 are the time constants [43] and the results are summarized in Table 3.

PBA was observed to have an average lifetime of 39 ns and this small lifetime can be due to a large concentration of the fluoroprobe. On coupling with HPG, lifetime increases to 66 ns which is almost double that of pure PBA. But the fluorescene intensity was observed to decrease considerably (Fig. 8). Although a decrease in lifetime is usually observed with fluorescence quenching, sometimes the reverse may happen. This is because the difference in properties of the excited state, indicating a high degree of aggregation of the dye on the dendritic platform. There are two main types of aggregation J- and H-aggregation. In the latter, the transition dipole moment becomes very low as a result of which fluorescence lifetime can become very long too. This aggregation behaviour is justified by the excimer peak in the PL spectrum of HPG-PBA conjugates (Fig. 8).

On doping with α-Fe_2O_3 nanoparticles, lifetime has no significant change but a slight decrease of about 2 ns (Table 2),

Table 3 Average lifetime calculation from TCSPC measurements

Sample	a_1	τ_1(ns)	a_2	τ_2(ns)	τ_{av}(ns)	Chi^2
PBA	1.88	5	98.12	39.79244	39	1.023032
HPG-PBA	−33.09	62.46321	133.09	50.08042	66	1.213098
HPG-PBA-IONP	2.14	2.32722	97.86	37.43198	36.67	1.157906

accompanied by almost complete quenching of PL emission. No considerable change in the fluorescence lifetime indicates a static quenching mechanism in which PBA and IONPs form a non-fluorescent complex before excitation. But the presence of a significant broad peak around 450–470 nm in the PL spectrum of HPG-PBA-IONP (Fig. 7) indicates the presence of excimers. To conclude, IONP doped sample undergoes a mixed static-dynamic quenching mechanism.

Conclusions

The present study focussed on the quenching mechanisms that prevail in pyrene butyric acid on a dendritic modification with hyperbranched polyglycerol and further doping with iron oxide nanoparticles which belongs to α-Fe_2O_3 phase. The FTIR and NMR spectra of the coupled products indicate the covalent interaction of the dendrimer and PBA through an ester linkage. Both HPG coupled and IONP doped products showed considerable decrease in PL emission confirming the presence of quenching. Both products showed an excimer emission around 450 nm, with a considerable decrease in monomer emission. On doping with α-Fe_2O_3 nanoparticles, PL emission corresponding to pyrene monomers almost completely get quenched and showed no fluorescent type of emission.

More insight into the quenching mechanism was drawn by means of fluorescent lifetime measurements with TCSPC technique. All the samples showed double exponential decay curves. An increase in lifetime of quenched HPG-PBA aggregates can be explained by H-aggregation. Thus the dendritic HPG was able to facilitate the aggregation of PBA molecules in a close proximity. IONP doped sample showed only a decrease of 2 ns in the lifetime when compared to pure PBA. This constancy in lifetime may be due to the presence of static quenching. But the presence of excimer as is clear from PL emission suggests the possibility of a mixed static-dynamic quenching to occur in the HPG-PBA-IONP sample.

Acknowledgements The authors acknowledge Prof. Holger Frey and his group, Johannes-Gutenberg University, Mainz, Germany. Also, the first author thanks University Grants Commission for Junior Research Fellowship (Sr.No-2061410045 Ref.No-22/06/2014 (i) EU-V).

References

1. Chen SH, Duhamel J, Bahun GJ, Adronov A (2011) Quantifying the presence of unwanted fluorescent species in the study of pyrene labelled macromolecules. J Phys Chem B 115(33):9921–9929
2. Chen RJ, Zhang YG, Wang DW, Dai H (2001) Noncovalent sidewall functionalization of single-walled carbon nanotubes for protein immobilization. J Am Chem Soc 123(16):3838–3839
3. Lakowicz JR (2006) Principles of fluorescence spectroscopy. 3rd edition. Springer
4. Zhao J, Ahlberg P, Hägglund C, Djurberg V, Scheicher RH, Zhang S, Zhang Z (2017) On monolayer formation of pyrenebutyric acid on graphene. Langmuir 33:3588–3593. https://doi.org/10.1021/acs.langmuir.6b04237
5. Kong N, Gooding JJ, Liu J (2014) Protein sensors based on reversible π-π stacking on basal plane HOPG electrodes. J Solid State Electrochem 18:3379–3386
6. Schneider GF, Xu Q, Hage S, Luik S, Spoor JNH, Malladi S, Zandbergen H, Dekker C (2013) Tailoring the hydrophobicity of graphene for its use as nanopores for DNA translocation. Nat Commun 4:2619
7. Singh M, Holzinger M, Tabrizian M, Winters S, Berner NC, Cosnier S, Duesberg GS (2015) Noncovalently functionalized monolayer graphene for sensitivity enhancement of surface plasmon resonance immunosensors. J Am Chem Soc 137:2800–2803
8. Wang M, Wang J, Wang F, Xia X (2012) The electrochemical properties of 1-pyrene butyricacid/graphene composites and their application in glucose biosensors. Journal of electrochemistry 18(5). Artical ID:1006–3471(2012)05–0450-07
9. Li X, Wang M, Tan H, Yang Q, Wang A, Bai L, Zhao H, Wu Y (2015) Preparation of the water-soluble pyrene-containing fluorescent polymer by one-pot method. Polymers 7:2625–2637. https://doi.org/10.3390/polym7121538
10. Ara AM, Iimori T, Yoshizawa T, Nakabayashi T, Ohta N (2006) External electric field effects on fluorescence of pyrene butyric acid in a polymer film: concentration dependence and temperature dependence. J Phys Chem B 110:23669–23677
11. Knopp J, Weber G (1867) Fluorescence depolarization measurements on pyrene butyric-bovine serum albumin conjugates. J Biol Chem 242(6):1353–1359
12. Duhamel J (2012) New insights in the study of pyrene excimer fluorescence to characterize macromolecules and their supramolecular assemblies in solution. Langmuir 28:6527–6538
13. Winnik MA (1985) End-to-end cyclization of polymer chains. Acc Chem Res 18:73–79
14. Birks JB (1970) Photophysics of aromatic molecules. Wiley, New York, p 301
15. Marcus RA, Sutin N (1985) Electron transfers in chemistry and biology. Biochim Biophys Acta 811:265–322
16. Vaughan WM, Weber G (1970) Oxygen quenching of pyrenebutyric acid fluorescence in water. Dynamic probe of the microenvironment. Biochemistry 9(3):464–473
17. Arndt-Jovin DJ, Latt SA, Stringkler G, Jovin TM (1979) Fluorescence decay analysis in solution and in a microscope of DNA and chromosomes stained with quinacrine. J Histochem Cytochem 27:87–95
18. Latt SA, Brodie S (1976) in: Excited States of Biological Molecules, Ed. J.B. Burks, Wiley New York pp:178
19. Winnik FM, Winnik MA, Tazuke S (1987) The synthesis and characterization of pyrene-labelled hydroxypropylcellulose and its fluroescence in solution. Macromolecules 20:38–44
20. Winnik FM (1987) Effect of temperature on aqueous solutions of pyrene-labeled (hydroxypropyl)cellulose. Macromolecules 20(11):2745–2750
21. Winnik FM (1989) Association of hydrophobic polymers in water: fluorescence studies with labeled (hydroxypropyl)celluloses. Macromolecules 22:734–742
22. Winnik FM (1990) Interaction of fluorescent dye labeled (hydroxypropyl)cellulose with nonionic surfactants. Langmuir 6:522–524
23. Fujiwara Y, Okurab I, Miyashitac T, Amaoa Y (2002) Optical oxygen sensor based on fluorescence change of pyrene-1-butyric acid chemisorption film on an anodic oxidation aluminium plate. Anal Chim Acta 471:25–32

24. Fraiji LK, David M, Werner TC (1992) Static and dynamic fluorescence quenching experiments for the physical chemistry laboratory. J Chem Educ 69(5):424
25. Jiang Z, Leppert V, Kelley DF (2009) Static and dynamic emission quenching in core/shell nanorod quantum dots with hole acceptors. J Phys Chem C 113(44):19161–19171
26. Ebenstein Y, Mokari T, Banin U (2002) Fluorescence quantum yield of CdSe/ZnS nanocrystals investigated by correlated atomic-force and single particle fluorescence microscopy. Appl Phys Lett 80:4033–4035
27. Förster T (1959) Transfer mechanisms of electronic excitation. Discuss Farady Soc 27:7–17
28. Hecht S, Fréchet JM (2001) Dendritic encapsulation of function: applying nature's site isolation principle from biomimetics to materials science. Angew Chem Int Ed 40(1):74–91
29. Tomalia DA, Baker H, Dewald J, Hall M, Kallos G, Martin S, Roeck J, Ryder J, Smith P (1985) A new class of polymers: starburst-dendritic macromolecules. Polym J 17:117–132
30. Newkome GR, Yao Z, Baker GR, Gupta VK (1985) Micelles. Part 1. Cascade molecules: a new approach to micelles. A [27]-arborol. J Org Chem 50(11):2003–2004
31. Alonso B, Moran M, Casado CM, Lobete F, Losada J, Cuadrado I (1995) Electrodes modified with electroactive films of organometallic dendrimers. Chem Mater 7:1440–1442
32. Abd-El-Aziz AS, Abdelghani AA, Wagner BD, Abdelrehim EM (2016) Aggregation enhanced excimer emission (AEEE) with efficient blue emission based on pyrene dendrimers. Polym Chem 7: 3277–3299. https://doi.org/10.1039/c6py00443a
33. Padghan SD, Bhosale RS, Bhosale SV, Antolasic F, Kobaisi M, Bhosale SV (2017) Pyrene-phosphonate conjugate: aggregation-induced enhanced emission, and selective Fe3+ ions sensing properties. Molecules 22:1417. https://doi.org/10.3390/molecules22091417
34. Neises B, Steglich W (1978) Simple method for the esterification of carboxylic acids. Angew Chem Int Ed Engl 17:522–524
35. Baykal A, Toprak MS, Durmus Z, Senel M, Sozeri H, Demir A (2012) Synthesis and characterisation of dendrimer-encapsulated iron and iron-oxide nanoparticles. J Supercond Nov Magn 25: 1541–1549
36. Pal B, Sharon M (2000) Preparation of iron oxide thin film by metal organic deposition from Fe(III)-acetylacetonate: a study of photocatalytic properties. Thin Solid Films 379:83–88
37. Xu YY, Zhao D, Zhang XJ, Jin WT, Kashkarov P, Zhang H (2009) Synthesis and characterization of single-crystalline α-Fe $_2$O $_3$ nanoleaves. Physica E: Low-dimensional Systems and Nanostructures 41:806–811
38. Darezereshki E (2011) One-step synthesis of hematite (α-Fe_2O_3) nano-particles by direct thermal-decomposition of maghemite. Mater Lett 65:642–645
39. Wang Y, La A, Bruckner C, Lei Y (2012) FRET- and PET-based sensing in a single material: expanding the dynamic range of an ultra-sensitive nitroaromatic explosives assay. Chem Commun 48: 9903–9905
40. Turro NJ, Ramamurthy V, Scaiano JC (2010) Modern molecular photochemistry of organic molecules, University Science Books, Sausalito, CA
41. Sunder A, Hanselmann R, Frey H, Mullhaupt R (1999) Controlled synthesis of hyperbranched polyglycerols by ring-opening multibranching polymerization. Macromoleccules 32:4240–4246
42. O'Connor DVO (1984) Phillips D. Time-correlated single photon counting. academic press, London
43. Morello G, Anni M, Cozzoli PD, Manna L, Cingolani R, De Giorgi M (2007) Picosecond Photoluminescence Decay Time in Colloidal Nanocrystals: The Role of Intrinsic and Surface States. J Phys Chem C 111:10541–10545